PHYSICAL REVIEW D

PARTICLES AND FIELDS

THIRD SERIES, VOLUME 36, NUMBER 7 1 OCTOBER 1987

Rho and omega production in $\pi^+ p$ interactions at 15.7 GeV/c

M. Ferguson,[a] T. Glanzman,[b] A. T. Goshaw, P. Lucas,[c] N. Morgan,[d]
W. Robertson, and W. D. Walker
Duke University, Durham, North Carolina 27706

P. M. Barlow,[e] R. K. Clark,[f] R. N. Diamond,[g] V. Hagopian, J. E. Lannutti, and C. M. Spencer[h]
Florida State University, Tallahassee, Florida 32306

W. Bugg, G. Condo, T. Handler, E. Hart, and A. Rogers[i]
University of Tennessee, Knoxville, Tennessee 37996

H. O. Cohn
Oak Ridge National Laboratory, Oak Ridge, Tennessee 37830

I. J. Kim and C. R. Sun
State University of New York at Albany, Albany, New York 12203

R. Gearhart
Stanford Linear Accelerator Center, Stanford, California 94305
(Received 10 February 1986; revised manuscript received 4 April 1987)

We report the results of a study of ρ and ω production in $\pi^+ p$ interactions at 15.7 GeV/c. The SLAC hybrid bubble-chamber facility was used to study reactions in which neutral particles are produced. Three tantalum plates inside the 40-in. bubble chamber and a large array of lead glass downstream of the chamber provided photon detection over a large solid angle. Final states with two neutral particles have been isolated with kinematic fits in which neutral pions were reconstructed in the plates and lead glass. Data from an earlier untriggered $\pi^+ p$ bubble-chamber experiment at 15 GeV/c were used to obtain samples of events in channels which did not trigger the hybrid system. Cross sections for ρ and ω production are given for several exclusive final states. Relative ρ and ω production rates are studied. The ratio of nondiffractive ω to ρ^0 production is measured to be $\omega/\rho^0 = 0.44 \pm 0.07$. We estimate the inclusive ω cross section to be 1.9 ± 0.3 mb. The results are compared to the Lund model of low-p_T hadronic reactions.

I. INTRODUCTION

In recent years many quark-parton models of low-p_T hadronic reactions have been developed.[1,2] The extension of parton ideas from hard constituent scattering to soft processes was motivated by similarities observed in the properties of leptonic jets and the "soft" jets produced in hadronic reactions. These observations raised the possibility of "jet universality" which explains the similarities by assuming that the particle production mechanism in leptonic interactions—parton hadronization—is also that for hadronic reactions. Models based on jet universality use the structure functions and fragmentation functions measured in leptonic reactions to simulate the parton hadronization process in hadron-hadron collisions. Tests of these models have most often involved studies of pseudoscalar-meson production. However, most of these particles are the decay products of meson resonances, and only a small fraction, perhaps as low as 10%, are produced directly.[3] The production dynamics are observed more directly in the systematics of vector-meson production. Unfortunately, the data for resonance production are more limited than those for pseudoscalar mesons; they are particularly limited for resonances which include a neutral particle among their decay products.

We report new results on ρ and ω production in $\pi^+ p$ interactions at a center-of-mass energy of 5.4 GeV.

Data were acquired with the SLAC hybrid-bubble-chamber facility which included an external photon detector. The ability to reconstruct π^0's allows the measurement of vector-meson production in exclusive final states with two neutral particles. These data were augmented with events from an untriggered 15-GeV/c π^+p bubble-chamber experiment. The combined data sample allowed a more comprehensive analysis than was previously possible.

The plan of the paper is as follows. Section II describes the experimental procedure. Section III presents the results for the relative ρ and ω cross sections and the inclusive ω cross section. In Sec. IV the predictions of the Lund model of low-p_T hadronic reactions are compared to the measurements. We summarize our results and present conclusions in Sec. V.

II. EXPERIMENTAL PROCEDURE

A. Data samples

The results reported here were obtained with data from two bubble-chamber experiments. The more recent data were obtained at the SLAC hybrid-bubble-chamber facility. The 40-in. bubble chamber was filled with hydrogen and exposed to a 15.7-GeV/c π^+ beam. A large array of lead glass was placed behind the chamber to provide photon detection. Three tantalum plates, each of one radiation length thickness, were mounted inside the bubble chamber to convert photons at large angles. The lead glass and the plates together, provided photon detection over 85% of 4π steradians in the center of mass for interactions occurring at the center of the chamber. The trigger required an energy deposition of 8 GeV in the lead glass. Final states with two neutral particles (e.g., π^0-π^0 or neutron-π^0) were isolated by kinematic fits in which one or two π^0's were reconstructed in the lead glass and plates. The details of the experimental arrangement and cross-section measurements are given elsewhere.[4–6] The production of ρ and ω mesons was studied in the following channels:

$$\pi^+p\to\pi^+p\pi^0\pi^0 , \tag{1}$$

$$\pi^+p\to\pi^+\pi^+n\pi^0 , \tag{2}$$

$$\pi^+p\to\pi^+p\pi^+\pi^-\pi^0 , \tag{3}$$

$$\pi^+p\to\pi^+p\pi^+\pi^-\pi^0\pi^0 , \tag{4}$$

$$\pi^+p\to\pi^+\pi^+\pi^+\pi^-n\pi^0 . \tag{5}$$

Data in other channels were obtained from a high-statistics 15-GeV/c π^+p experiment of Baltay *et al.*[7] The data-summary tapes from this untriggered bubble-chamber experiment were obtained and event samples from the following reactions isolated:

$$\pi^+p\to\pi^+p\pi^+\pi^- , \tag{6}$$

$$\pi^+p\to\pi^+p\pi^+\pi^+\pi^-\pi^- , \tag{7}$$

$$\pi^+p\to\pi^+p\pi^+\pi^+\pi^-\pi^-\pi^0 , \tag{8}$$

plus data on reaction (3). The details of the data reduction and cross-section determinations for these reactions are given in Ref. 7. Table I lists the number of events used in this analysis for each of the reactions (1)–(8).

TABLE I. Number of events.

Reaction	Number of events
$\pi^+p\to\pi^+p\pi^0\pi^0$	5 163
$\pi^+p\to\pi^+\pi^+n\pi^0$	750
$\pi^+p\to\pi^+p\pi^+\pi^-\pi^0$	1 277 (triggered data)
	16 269 (untriggered data)
$\pi^+p\to\pi^+p\pi^+\pi^-\pi^0\pi^0$	3 404
$\pi^+p\to\pi^+\pi^+\pi^+\pi^-n\pi^0$	1 355
$\pi^+p\to\pi^+p\pi^+\pi^-$	24 803
$\pi^+p\to\pi^+p\pi^+\pi^-\pi^-$	7 136
$\pi^+p\to\pi^+p\pi^+\pi^+\pi^-\pi^-\pi^0$	10 090

B. Resonance fitting

The cross sections for ρ and ω production have been measured in each of the channels listed above. The amount of resonance production in the two-pion and three-pion invariant-mass distributions was measured as follows.

The number of particles in a resonance peak was determined with a χ^2 minimization fit of the following function to the invariant-mass distribution[8]

$$d\sigma/dm = B + PR . \tag{9}$$

The functions B, P, and R describe the background, phase space, and resonance structure, respectively. In practice, it was assumed that the phase space and background distributions have the same mass dependence, and P in the above equation has been replaced by $a_R B$, where a_R is the intensity of the resonance relative to the background. The regions above and below the two-pion mass at which the ρ background peaked were described by separate equations. The region below the peak mass was fit with a third-order polynomial. The background beyond the peak was taken to have an exponential form:

$$B(m) = A\exp(-bm - cm^2) .$$

The ρ resonance was described by a relativistic p-wave Breit-Wigner function.[9] Additional resonance terms were added to (9) to include the f and g mesons when necessary.

A second-order polynomial was used to describe the background under the ω peak in the $\pi^+\pi^-\pi^0$ mass distribution. The ω resonance was fit with a simple Breit-Wigner function which was convoluted with a Gaussian mass resolution distribution. The widths and masses of the resonances were fixed at the values given in the Particle Data Group Tables:[10]

$$m_\rho = 769\ \text{MeV},\quad m_\omega = 783\ \text{MeV} ,$$

$$\Gamma_\rho = 154\ \text{MeV},\quad \Gamma_\omega = 9.9\ \text{MeV} .$$

All other parameters were determined by the fit. The ω

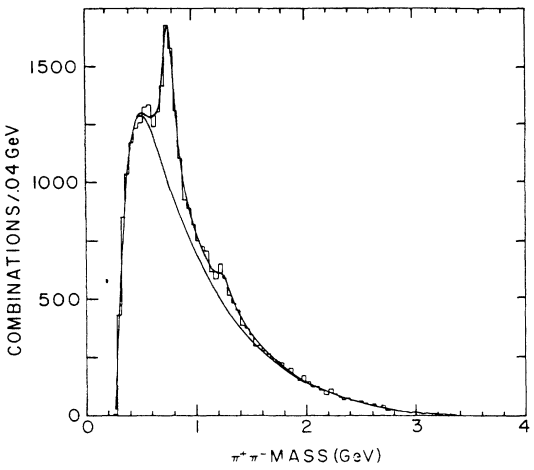

FIG. 1. Fit of Eq. (9) to the $\pi^+\pi^-$ invariant-mass distribution for $\pi^+p \to \pi^+p\pi^+\pi^-\pi^0$. The lower curve is the background as determined by the fit.

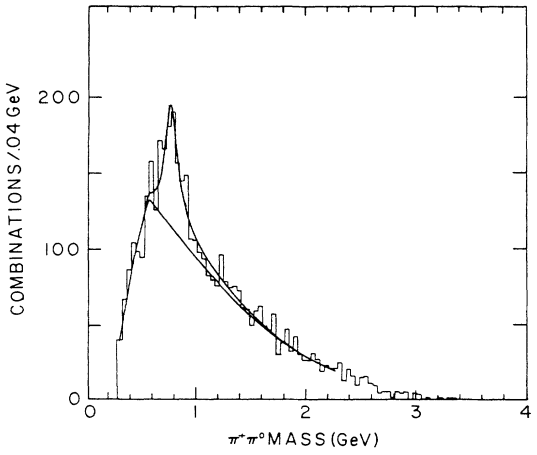

FIG. 3. Fit of Eq. (9) to the $\pi^+\pi^0$ invariant-mass distribution for $\pi^+p \to \pi^+\pi^+n\pi^0$. The lower curve is the background as determined by the fit.

fits were done over the mass range from 0.6 GeV/c^2 to 1.2 GeV/c^2. The ρ-meson fits extended from threshold to an upper limit determined by the number of events. For the most populated channels, fits to 2.5 GeV/c^2 and beyond were done. In channels with less events the upper limit was chosen to exclude bins with populations of 10 counts or less. The mass range extended to at least 1.5 GeV/c^2 for all ρ fits.

A fit with a χ^2 per degree of freedom less than 1.5 was obtained for each of the ρ and ω channels. In each case the full distribution and background distribution were plotted against the data and checked for reasonableness. The mass resolution as determined by the ω fits was 10–20 MeV for the untriggered data and 20–30 MeV for the hybrid experiment. Examples of a typical fit are shown in Figs. 1–4. Figures 1 and 2 show the results for the ρ^0 and ω in the $\pi^+p\pi^+\pi^-\pi^0$ events of Ref. 7. Figures 3 and 4 show the fit to the ρ^+ in the $\pi^+\pi^+n\pi^0$ and $\pi^+p\pi^0\pi^0$ channels, respectively.

C. Cross-section calculations

The numbers of particles in the resonance structure determined by the fits were used to calculate the cross sections for the ρ and ω channels. For the untriggered data [reactions (6)–(8)], the resonance cross section was taken as the fraction of the total final-state cross section given by the ratio of the number of resonance particles to the total number of events.

Cross sections for the hybrid data were calculated with a normalization relation determined from samples of untriggered data.[4] Corrections for acceptance and trigger efficiency were determined with a computer model of the hybrid facility. The data from the untriggered

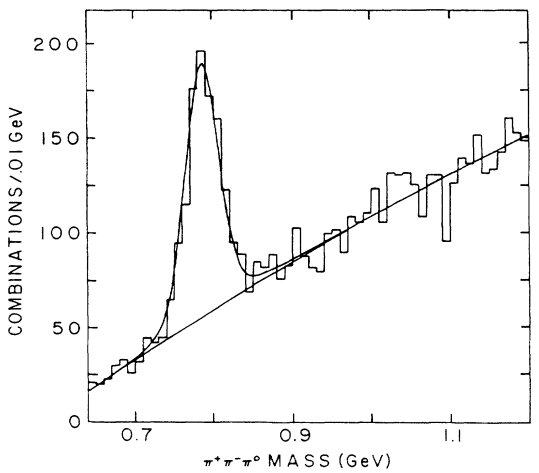

FIG. 2. Fit of Eq. (9) to the $\pi^+\pi^-\pi^0$ invariant-mass distribution for $\pi^+p \to \pi^+p\pi^+\pi^-\pi^0$. The lower curve is the background as determined by the fit.

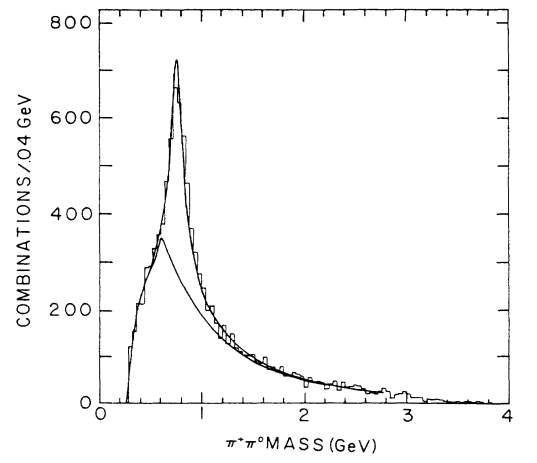

FIG. 4. Fit of Eq. (9) to the $\pi^+\pi^0$ invariant-mass distribution for $\pi^+p \to \pi^+p\pi^0\pi^0$. The lower curve is the background as determined by the fit.

experiment were used to obtain an unbiased sample of events with which the efficiencies were evaluated. For example, events of the type $\pi^+\pi^-\to\pi^+p\pi^0\pi^0\rho^0$ were simulated with the $\pi^+p\to\pi^+p\pi^+\pi^+\pi^-\pi^-$ events obtained from the data-summary tapes of Ref. 7. One $\pi^+\pi^-$ pair was taken to be a $\pi^0\pi^0$ pair and a cut requiring the invariant mass of another $\pi^+\pi^-$ pair be in the ρ mass region was applied. The acceptance for the channel was taken as the fraction of the selected events which satisfied the trigger requirements as applied with the computer model. An acceptance of (46±10)% was determined for this channel. A similar procedure was used to measure the acceptance of other ρ and ω channels.

Additional studies of the trigger efficiency were done with samples of data taken without the trigger in effect. The overall acceptance for four-prong events was found to increase from 46% to 63% as the energy carried by π^0's increased from 2 to 15 GeV. However, the acceptance diminished rapidly as the neutral energy decreased below 2 GeV. Therefore, a cut was made requiring the neutral energy be greater than 2 GeV and the four-prong results are quoted as partial cross sections.

TABLE II. Resonance-production cross sections.

Reaction	Cross section[a] (μb)
$\pi^+p\to\pi^+p\rho^0$	673±27
$\pi^+p\to\pi^+n\rho^+$	150±41
$\pi^+p\to p\pi^0\rho^+$	356±95
$\pi^+p\to\pi^+p\omega$	51.3±4.7
$\pi^+p\to\pi^+p\pi^0\rho^0$	73±18[b]
$\pi^+p\to\pi^+p\pi^-\rho^+$	151±16
$\pi^+p\to\pi^+p\pi^+\rho^-$	53±8.6
$\pi^+p\to\pi^+p\pi^0\omega$	125±35[b]
$\pi^+p\to\pi^+p\pi^0\pi^0\rho^0$	91±34[b]
$\pi^+p\to\pi^+p\pi^-\pi^0\rho^+$	263±80[b]
$\pi^+p\to\pi^+p\pi^+\pi^0\rho^-$	88±34[b]
$\pi^+p\to\pi^+\pi^+\pi^0n\rho^0$	69±29[b]
$\pi^+p\to\pi^+\pi^+\pi^-n\rho^+$	128±46[b]
$\pi^+p\to\pi^+\pi^+\pi^+n\rho^-$	15±11[b]
$\pi^+p\to\pi^+\pi^+n\omega$	40±19[b]
$\pi^+p\to\pi^+\pi^+n\rho^0$	162±28
$\pi^+p\to\pi^+p\pi^+\pi^-\rho^0$	330±15
$\pi^+p\to\pi^+p\pi^+\pi^-\omega$	81±9
$\pi^+p\to\pi^+p\pi^+\pi^-\pi^0\rho^0$	323±31
$\pi^+p\to\pi^+p\pi^+\pi^-\pi^-\rho^+$	98±15
$\pi^+p\to\pi^+p\pi^+\pi^+\pi^-\rho^-$	35±11

[a]The ω cross sections have been corrected to allow for all decay modes.

[b]This cross section is for events with E_{π^0} or $E_{\pi^0\pi^0}$ greater than 2 GeV and proton momentum less than 1.5 GeV/c or neutron momentum less than 2 GeV/c.

III. CROSS SECTIONS AND RELATIVE ω AND ρ PRODUCTION RATES

A. ρ and ω cross sections

The cross sections of the ρ and ω channels in reactions (1)–(8) are given in Table II.[11] Separate measurements of the cross sections from reaction (3) were made with the data from each experiment. The results were in agreement except for the reaction

$$\pi^+p\to\pi^+p\pi^0\rho^0 \ . \tag{10}$$

In this channel the resonance did not allow one to discriminate against multineutral background as in cases where the π^0 is required to be in a mass combination in the resonance region. Since the events in the untriggered data were selected on the basis of one-constraint fits, the background contamination is much worse than in the hybrid experiment which used the lead glass to detect π^0's. This issue is discussed in detail in Ref. 5. The results reported here for resonance production in reaction (3) are taken from the analysis of the untriggered data, excepting reaction (10) for which the results of the hybrid experiment are given. In this way the benefits of the high statistics and good acceptance of the untriggered experiment are obtained in the channels without severe background problems.

B. ρ^0 and ω cross sections and relative production rates

The ratio of the ω and ρ^0 production rates was measured by comparing the cross sections of final states in which the kinematics are similar for the ρ^0 and ω. Table III lists the pairs of reactions that were used and their cross sections. The ratio of the full set of cross sections is

$$\omega/\rho^0=0.26\pm0.03 \ .$$

This ratio includes the effect of the large $\pi^+p\rho^0$ diffractive cross section. In general, models of low-p_T reactions do not include such diffractive components

TABLE III. Cross sections for ρ^0 and ω production in pairs of kinematically similar reactions.

Reaction	Cross section (μb) $M^0=\rho^0$	$M^0=\omega$
$\pi^+p\to\pi^+pM^0$	673±27	51.3±4.7
$\pi^+p\to\pi^+p\pi^0M^0$	73±18	125±35
$\pi^+p\to\pi^+\pi^+nM^0$	162±28	40±35
$\pi^+p\to\pi^+p\pi^+\pi^-M^0$	330±15	81±9
$\pi^+p\to\pi^+p2(\pi^+\pi^-)M^0$	76±15[a]	22±6[a]
$\pi^+p\to\pi^+p3(\pi^+\pi^-)M^0$	29±6[b]	24±7[c]

[a]This cross section was taken from Ref. 7.

[b]This cross section was taken from Ref. 12.

[c]This cross section was taken as one-half the value reported in Ref. 12 (see Sec. III B).

since their connection to constituent interactions is not understood. A ratio more relevant to the models is obtained by excluding the first pair of cross sections:

$$\omega/\rho^0 = 0.44 \pm 0.07 \ .$$

The only previous measurement at this energy obtained a value of 0.9 ± 0.15 for this ratio.[12] Our analysis includes two channels more than the earlier measurement since we can observe ω production in the π^0-π^0 and neutron-π^0 four-prong events. However, the difference between the two measurements is primarily due to a systematic discrepancy in the ω cross sections. The ω cross sections determined from both sets of our data are smaller by about a factor of 2 than those given in Ref. 12.

The naive prediction of quark models for this ratio is 1.0 since the quark constituents of the ρ^0 and ω are identical. We interpret the smaller value as evidence of ω suppression in the vector-meson production dynamics. Such a suppression may be attributed to two causes. First, the large one-pion-exchange cross sections favor ρ over ω production. This is due to the fact that the $\pi\pi$ vertex couples more strongly to the ρ and to states decaying to a ρ than to the ω. Second, the production rate of a given meson resonance is likely to depend linearly on the hadronic width of the resonance. Such an effect would result in ω suppression since $\Gamma_\omega/\Gamma_{\rho^0} \simeq 1/15$. Evidence of such a dependence is found in the observation that inclusive vector-meson cross sections in pp collisions at higher energies depend linearly on the resonance width.[13]

We have investigated the relative strength of the two suppression effects by measuring the ω/ρ^0 ratio in the central and fragmentation regions. The central region is taken to include resonances with Feynman x between zero and 0.5. Only the forward central region was considered because of the low trigger acceptance for ω's produced backward in the center of mass. Resonances with x greater than 0.5 are considered to be in the fragmentation region. The ratio in the fragmentation region is representative of the suppression related to the $\pi\pi$ vertex since exchange reactions are highly peripheral. The ratio in the central region is more sensitive to the width-dependent effect. Mesons produced in this region are thought to originate from a quark-antiquark sea which is produced at small x by the interacting quarks. A width dependence in the dynamics of particle production will be reflected in the ratios of mesons produced as hadrons condense from the sea. The ratios in the central and fragmentation regions were measured to be 0.41 ± 0.08 and 0.42 ± 0.09, respectively. Thus, the ω suppression occurs with equal strength in the central and fragmentation regions.

C. Inclusive ω cross section

A direct measurement of the inclusive ω cross section is difficult to make because all charged and neutral pions would have to be reconstructed. However, the cross section can be estimated as follows.

The reactions in Table III account for nearly 30% of the inclusive ρ^0 cross section, and it is likely that a similar fraction of the inclusive ω cross section is represented. All the significant topologies are present and results from multineutral reactions are included. It is therefore reasonable to take the ω/ρ^0 ratio in these reactions as an estimate of the fully inclusive ratio. The inclusive ω cross section can then be obtained by scaling the inclusive ρ^0 cross section by the estimated ω/ρ^0 ratio. However, the contribution of the diffractive $\pi^+p\rho^-$ channel must first be subtracted from the ρ^0 cross section since the ω g parity does not allow a similar large cross section for the ω. The $\pi^+p\omega$ cross section is added back to the scaled cross section. Thus

$$\sigma_\omega = (\sigma_{\rho^0} - \sigma_{\pi^+p\rho^0})(\sigma_\omega/\sigma_{\rho^0})_{\text{estimated}} + \sigma_{\pi^+p\omega}$$
$$= 1.9 \pm 0.3 \text{ mb} \ .$$

The value of $\sigma_{\rho^0} = 4.8 \pm 0.4$ reported in Ref. 8 was used. The previous estimate of $\sigma_\omega = 4.0 \pm 0.7$ mb reported in Ref. 12 used a larger ω/ρ^0 ratio (see Sec. III B) and did not remove the $\sigma_{\pi^+p\rho^0}$ cross section for σ_{ρ^0} before scaling.

D. Relative production rates of ρ^+, ρ^-, and ρ^0

The relative production rates of the three charge states of the ρ were measured by comparing the cross sections of four reactions for each of the ρ charge states. Table IV lists the reactions and the cross sections. The results are given for the central and fragmentation regions (as defined in Sec. III B) in order to exhibit more clearly the effects of the quark flow from the beam to the ρ. These cross sections were measured with mass distributions obtained by selecting particle combinations

TABLE IV. Cross sections for ρ^0, ρ^+, and ρ^-.

	Cross section (μb) in x bins					
	$(\pi\rho)^0 = \pi^0\rho^0$		$(\pi\rho)^0 = \pi^-\rho^+$		$(\pi\rho)^0 = \pi^+\rho^-$	
Reaction	$0 < x < 0.5$	$0.5 < x < 1$	$0 < x < 0.5$	$0.5 < x < 1$	$0 < x < 0.5$	$0.5 < x < 1$
$\pi^+p \to \pi^+p(\pi\rho)^0$	40 ± 11	27 ± 10	58 ± 7	84 ± 8	25 ± 5	12 ± 4
$\pi^+p \to \pi^+p\pi^0(\pi\rho)^0$	74 ± 27	8 ± 8	122 ± 42	162 ± 45	89 ± 32	12 ± 9
$\pi^+p \to \pi^+\pi^+n(\pi\rho)^0$	36 ± 16	7 ± 8	49 ± 25	64 ± 20	4 ± 9	9 ± 4
$\pi^+p \to \pi^+p\pi^+\pi^-(\pi\rho)^0$	179 ± 17	52 ± 6	57 ± 11	24 ± 5	23 ± 9	9 ± 4
Total	329 ± 37	94 ± 16	286 ± 50	334 ± 50	141 ± 35	42 ± 12

TABLE V. Measured ρ cross-section ratios and Lund-model predictions.

	Central region $(0<x<0.5)$		Fragmentation region $(x>0.5)$	
Ratio	Measured	Lund	Measured	Lund
ρ^-/ρ^+	0.49±0.15	0.38±0.01	0.13±0.04	0.05±0.002
ρ^0/ρ^+	1.15±0.24	1.05±0.02	0.28±0.11	0.15±0.01
ρ^-/ρ^0	0.43±0.12	0.36±0.01	0.45±0.15	0.33±0.01

which satisfied the x cuts. The methods described in Sec. II were used to count the numbers of resonance particles and calculate acceptance corrected cross sections. As with the full distributions, a good fit with χ^2 per degree of freedom less than 1.5 was obtained and plotted against the data in each case.

Table V gives the ratios determined from the results in Table IV. The relative sizes of the cross sections in the fragmentation region are consistent with the idea that these mesons are produced by leading quarks from the beam:

$$\sigma_{\rho^+} > \sigma_{\rho^0} > \sigma_{\rho^-} .$$

The ratios in the central region also exhibit a dependence on the beam valence quarks since both flavors of the beam quarks are common to ρ^+ and ρ^0 but neither are in the ρ^-:

$$\sigma_{\rho^+} \simeq \sigma_{\rho^0} > \sigma_{\rho^-} .$$

This observation can be interpreted as evidence of the "held back" quark effect which postulates that one of the beam quarks is held back in the central region while the other fragments with a large fraction of the full beam momentum.[14]

IV. COMPARISON WITH THE LUND MODEL

A. The Lund model of low-p_T hadronic collisions

The confinement property of quantum chromodynamics (QCD) suggests that the color force can be simulated with a string model. The Lund model of quark fragmentation combines semiclassical string dynamics with elements of QCD to simulate jet production in electron-positron annihilation.[15–17] Hadronization in this formulation is most easily treated as a stochastic process, and a Monte Carlo program is used to obtain the predictions of the model. The success achieved with leptonic reactions prompted the extension of the model to low-p_T hadron-hadron collisions. Since the predictions for hadronic reactions are also obtained from Monte Carlo–generated events, they may be tested in specific channels. Thus, unlike other models which only predict inclusive distributions, the Lund model can be compared to data for mesons which are difficult to study inclusively (e.g., ω, ρ^+, ρ^-).

The extension of the model from the relatively simple quark-antiquark configuration in electron-positron annihilation to the complexities of hadron-hadron collisions required the assumption of a reasonable mechanism whereby the hadronic reactions proceed. The authors of the model postulated that the hadronic processes occur as follows. The color field of a quark in the beam overlaps with that from a target quark such that these quarks expend all their energy in stretching the color flux tube between them. The remaining quarks move into their respective hemispheres until their energy is also contained in the color field. The final configuration is a single color flux tube with all five valence quarks located at various positions along the tube. The structure functions of the incoming hadrons are used to determine which pair of valence quarks interact initially and the locations of the quarks along the color field. The Lund fragmentation scheme is used to hadronize the stretched system into a hadronic final state.

In the following sections the predictions of the Lund model are compared to the ρ and ω measurements reported above. A total of 200 000 $\pi^+ p$ interactions at a center-of-mass energy of 5.4 GeV were generated with the Lund Monte Carlo program. These events were analyzed just as the real data to obtain the model's predictions for relative cross sections and Feynman-x distributions.

B. Relative cross sections for ρ and ω final states

The Lund-model prediction of the cross sections of several ρ and ω final states was obtained by counting the channel populations in the sample of Monte Carlo events. A sensitivity (in μb/event) for the Lund data was determined by a χ^2 fit which minimized the overall deviation of the predicted cross sections from the measured ones. Table VI lists the ρ and ω final states, the measured cross sections, and the Lund predictions (channels such as $\pi^+ p \rho^0$ which are dominated by diffractive processes are not included). Double-resonance production is included in the cross sections (e.g., the $\pi^+ p \rho^+ \rho^-$ channel adds to both the $\pi^+ p \pi^+ \pi^0 \rho^-$ and the $\pi^+ p \pi^- \pi^0 \rho^+$ cross sections).

The model agrees qualitatively with the data in that it reproduces the gross features of the cross sections. Some of the discrepancies are due to the absence of diffractive dissociation in the model. For instance, the low prediction for the $\pi^+ p \pi^+ \pi^- \rho^0$ channel is due to the contribution of beam and target dissociation, $\pi^+ \rightarrow A_1{}^+ \rightarrow \pi^+ \rho^0$ and $p \rightarrow p \pi^+ \pi^-$, respectively. Furthermore, since the only mesons included in the model are the pseudoscalar and vector multiplets, the contribution of tensor mesons to the ρ and ω cross sections is not included.

TABLE VI. Measured cross sections and Lund predictions for ρ and ω final states.

Reaction	Cross section (μb) Measured	Predicted
$\pi^+p\to\pi^+p\pi^0\rho^0$	73±18	106
$\pi^+p\to\pi^+p\pi^-\rho^+$	151±16	241
$\pi^+p\to\pi^+p\pi^+\rho^-$	53±8.6	58
$\pi^+p\to\pi^+p\pi^0\omega$	125±35	201
$\pi^+p\to\pi^+\pi^+n\omega$	40±19	21
$\pi^+p\to\pi^+\pi^+n\rho^0$	162±28	65
$\pi^+p\to\pi^+p\pi^0\pi^0\rho^0$	91±34	153
$\pi^+p\to\pi^+p\pi^-\pi^0\rho^+$	263±80	458
$\pi^+p\to\pi^+p\pi^+\pi^0\rho^-$	88±34	102
$\pi^+p\to\pi^+\pi^+\pi^0n\rho^0$	69±29	52
$\pi^+p\to\pi^+\pi^+\pi^-n\rho^+$	128±46	57
$\pi^+p\to\pi^+\pi^+\pi^+n\rho^-$	15±11	7
$\pi^+p\to\pi^+p\pi^+\pi^-\rho^0$	330±15	88
$\pi^+p\to\pi^+p\pi^+\pi^-\omega$	81±9	90
$\pi^+p\to\pi^+p\pi^+\pi^-\pi^0\rho^0$	323±31	194
$\pi^+p\to\pi^+p\pi^+\pi^-\pi^-\rho^+$	98±15	63
$\pi^+p\to\pi^+p\pi^+\pi^+\pi^-\rho^-$	35±11	15

The charge dependence of the ρ cross sections is reproduced rather well by the model. This dependence is displayed in more detail by Table V which gives the ρ^+, ρ^-, and ρ^0 cross-section ratios for the reactions listed in Table IV. The Lund-model predictions for these ratios are also shown. The impact of the beam valence quarks on the identity of forwardly produced mesons is evident in the numbers. The region with x_ρ greater than one-half is particularly sensitive to the beam quark flow. The model is in agreement with the data in the central region. The predictions for the fragmentation region are surprisingly good considering the large diffractive contribution to this region.

As expected, the Lund-model prediction for the ω/ρ^0 ratio was equal to 1.0 for the channels in Table III. However, when the data cuts on the π^0 momentum were applied to the Lund events, a ratio of $\omega/\rho^0=1.21\pm0.02$ was obtained. This result implies that the fully inclusive ω/ρ^0 ratio is less than the value of $0.44+0.07$ measured for our detected events. Using the Lund model to correct for the effect of the data cuts yields a ratio of $\omega/\rho^0=0.36\pm0.06$.

C. Feynman-x distributions

The ρ and ω Feynman-x distributions for the channels listed in Table II were compared to Lund-model predictions. As expected, the Lund events exhibited more central production relative to the fragmentation region than the data. However, this difference is not entirely due to diffractive processes. A sizable fraction of the inelastic π^+p cross section at this energy results from one-particle-exchange reactions. The presence of a strong Δ^{++} signal in these data indicates a large exchange component. The Lund data, however, exhibit very little Δ^{++} production and do not simulate well the peripheral nature of the exchange process. Presumably the constituent interaction mechanism which the model attempts to describe is revealed when the diffractive and exchange processes are removed. The peripheral events were eliminated in the following manner.

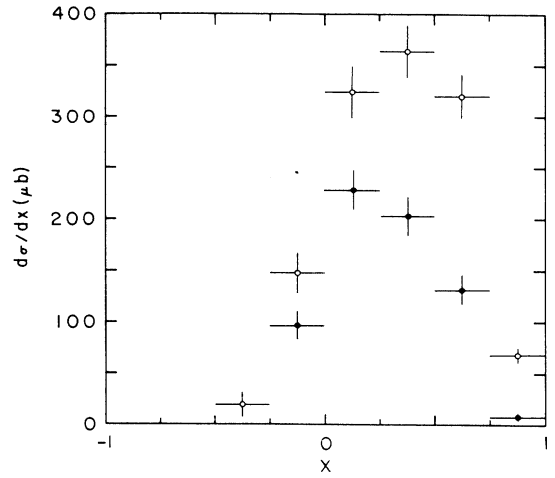

FIG. 5. $d\sigma/dx$ of the ρ^0 in $\pi^+p\to\pi^+p\pi^+\pi^+\pi^-\pi^-$ for all events (○) and after making longitudinal-phase-space cuts (●).

A feature of hadronic interactions is that the longitudinal-momentum distributions of final-state particles are sensitive to the particle-production dynamics.[18] We devised longitudinal-phase-space (LPS) cuts for several channels which removed the diffractive and exchange components. These cuts eliminated the LPS regions which are dominated by beam and target dissociation and quasi-two-body-exchange reactions. An example of the effect of the cuts on the Feynman-x distributions is shown in Fig. 5. The details of the LPS analysis

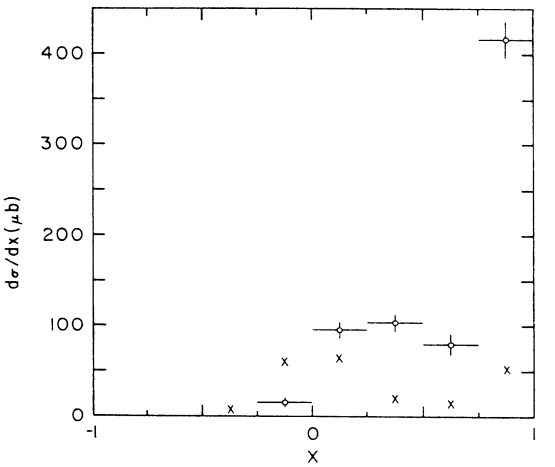

FIG. 6. $d\sigma/dx$ of ρ^0's in the reaction $\pi^+p\to\pi^+p\pi^+\pi^-$. The data points are given by the circles and the Lund-model prediction is shown with the x's.

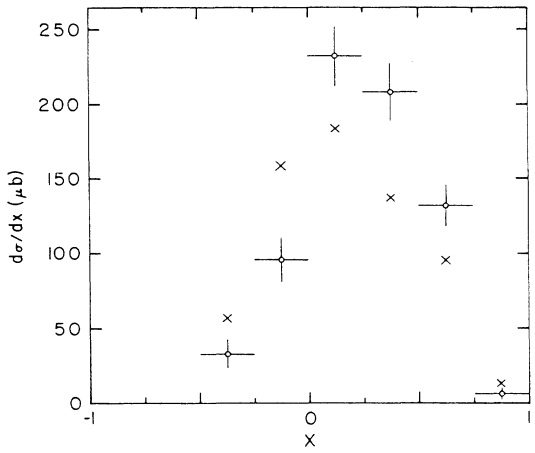

FIG. 7. $d\sigma/dx$ of ρ^0's in the reaction $\pi^+p\to\pi^+p\pi^+\pi^+\pi^-\pi^-$. The data points are given by the circles and the Lund-model prediction is shown with the x's.

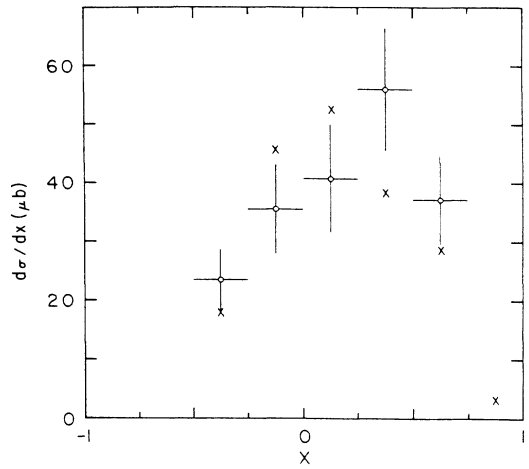

FIG. 9. $d\sigma/dx$ of ω's in the reaction $\pi^+p\to\pi^+p\pi^+\pi^+\pi^-\pi^-\pi^0$. The data points are given by the circles and the Lund-model prediction is shown with the x's.

are given in the Appendix.

Four examples of $d\sigma/dx$ distributions after making the LPS cuts are shown in Figs. 6–9. The predictions of the Lund model are also shown. Each Lund distribution was normalized to the data by a separate χ^2 fit. Ideally, the four normalization factors would have been the same, but, as discussed above, the model can only make qualitative predictions of relative channel cross sections. Since the general shape of the distributions is determined by kinematics, the agreement with regard to gross features does not imply that the dynamics are well simulated by the model. Rather, the salient feature is that the predicted distributions are more central than the observed ones.

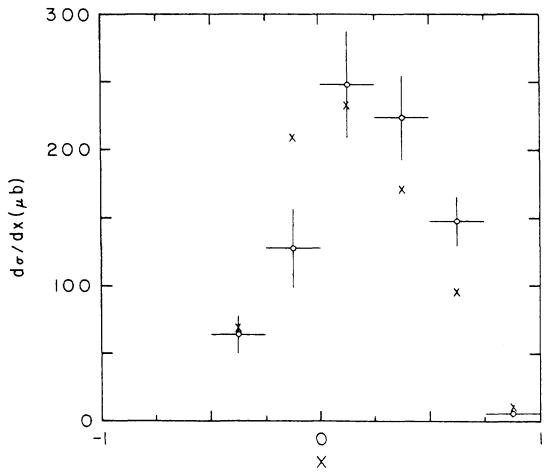

FIG. 8. $d\sigma/dx$ of ρ^0's in the reaction $\pi^+p\to\pi^+p\pi^+\pi^+\pi^-\pi^-\pi^0$. The data points are given by the circles and the Lund-model prediction is shown with the x's.

D. Interpretation

The results of tests of the Lund model given here and elsewhere present somewhat of a paradox.[19] The model successfully predicts relative particle yields in various kinematic regions (excepting ω production which involves some dynamic effects associated with the small width of the ω which are not included in the model), yet the predictions for channel cross sections and Feynman-x distributions find only qualitative agreement with the data. The following discussion presents our interpretation of what these observations imply about the dynamics of hadronic reactions.

The channel cross sections depend in a complex way on the distributions of the numbers of the various hadrons produced. These distributions are related to the number of color fields produced in the interactions and the amount of energy transferred to the fields. Obviously, the Feynman-x distributions also depend on the dynamics of the color field formation. The model's assumption of a single color flux tube to which the valence quarks transfer all their energy is certainly too simplistic to capture the full range of dynamic possibilities. However, since this configuration is likely to occur rather frequently, one would expect the qualitative agreement achieved by the model.

On the other hand, the relative particle yields are sensitive to the hadronization or "decay" of the color fields and are rather insensitive to the manner in which the fields are formed and stretched. The Lund model describes the hadronization process well since it was tuned to electron-positron annihilation in which parton hadronization can be cleanly observed. If the underlying particle-production mechanism in hadronic reactions, whether diffractive, exchange, or constituent scattering, is indeed this process, then the model's predictions of particle ratios should be correct even for regions dominated by peripheral processes. The model's success in

this regard implies that parton hadronization is the particle-production mechanism in hadronic collisions.

V. SUMMARY AND CONCLUSIONS

We have studied ρ and ω production in π^+p interactions with a hybrid bubble-chamber facility which included a lead-glass photon spectrometer. The π^0 detection provided by this apparatus allowed the measurement of several ρ and ω cross sections in exclusive reactions with two neutral final-state particles. We measure the ratio of ω to ρ^0 production to be $\omega/\rho^0=0.26\pm0.03$ for all observed channels and 0.44 ± 0.07 for nondiffractive production. This ratio is quite different from the value of 1.0 predicted by constituent-quark models. We interpret the smaller value as evidence of a width dependence in the vector-meson production dynamics. We estimate an inclusive ω cross section of 1.9 ± 0.3 mb by scaling from the measured inclusive ρ^0 cross section. The ratios of the production rates of ρ^+, ρ^-, and ρ^0 measured in the central and fragmentation regions are observed to follow the general trends predicted by quark models.

We have compared our measurements to the Lund model of low-p_T hadronic interactions. The model's predictions of the ρ production ratios are in quantitative agreement with the measurements. However, the model achieves only qualitative success with relative channel cross sections and Feynman-x distributions, even when diffractive and one-particle-exchange reactions are removed. We conclude that despite the model's other failings, its ability to predict particle-production ratios supports the hypothesis that parton hadronization is the particle-production mechanism in soft hadronic reactions.

ACKNOWLEDGMENTS

We thank the SLAC bubble-chamber group for their assistance in acquiring the data. We acknowledge the efforts of the scanning and measuring staffs at each of our laboratories. Dr. T. Sjöstrand provided the Lund Monte Carlo program. The high-energy physics group at Columbia University provided data-summary tapes from their experiment. This work was supported in part by grants from the U.S. Department of Energy.

APPENDIX

Longitudinal-phase-space cuts were used to remove the diffractive and one-particle-exchange components in the reactions

TABLE VII. Longitudinal-phase-space regions in which cuts were made to remove events produced by diffractive and exchange processes.

Final state	Forward particles	Backward particles	Events removed	Peripheral process removed
$\pi^+p\pi^+\pi^-$	π^+	$p\pi^+\pi^-$	All events	Target dissociation
$\pi^+p\pi^+\pi^-$	$\pi^+\pi^-$	$p\pi^+$	Events in which the mass of the backward π^+ and proton is less than 1.4 GeV/c^2	Exchange reaction in which a Δ^{++} is produced
$\pi^+p\pi^+\pi^-$	$\pi^+\pi^+\pi^-$	p	Events with the Feynman x of the forward $\pi^+\pi^+\pi^-$ combination greater than 0.88	A_1 and A_2 production
$\pi^+p\pi^+\pi^+\pi^-\pi^-$	$\pi^+\pi^-$	$p\pi^+\pi^+\pi^-$	All events	Exchange reactions
$\pi^+p\pi^+\pi^+\pi^-\pi^-$	$\pi^+\pi^+\pi^-$	$p\pi^+\pi^-$	Events with the Feynman x of the forward $\pi^+\pi^+\pi^-$ combination greater than 0.75	A_1 and A_2 production
$\pi^+p\pi^+\pi^+\pi^-\pi^-$	$\pi^+\pi^+\pi^-\pi^-$	$p\pi^+$	Events in which the mass of the backward π^+ and proton is less than 1.4 GeV/c^2	Exchange reaction in which a Δ^{++} is produced
$\pi^+p\pi^+\pi^+\pi^-\pi^-\pi^0$	$\pi^+\pi^-\pi^0$	$p\pi^+\pi^+\pi^-$	All events	Exchange reactions
$\pi^+p\pi^+\pi^+\pi^-\pi^-\pi^0$	$\pi^+\pi^+\pi^-\pi^0$	$p\pi^+\pi^-$	All events	Exchange reactions
$\pi^+p\pi^+\pi^+\pi^-\pi^-\pi^0$	$\pi^+\pi^+\pi^-\pi^-\pi^0$	$p\pi^+$	Events in which the mass of the backward π^+ and proton is less than 1.4 GeV/c^2	Exchange reaction in which a Δ^{++} is produced

$$\pi^+ p \to \pi^+ p \pi^+ \pi^- ,$$
$$\pi^+ p \to \pi^+ p \pi^+ \pi^+ \pi^- \pi^- ,$$
$$\pi^+ p \to \pi^+ p \pi^+ \pi^+ \pi^- \pi^- \pi^0 .$$

The LPS regions for each reaction were defined by the sets of particles which were forward and backward in the center of mass. For example, the $\pi^+ p \pi^+ \pi^-$ channel has five LPS regions corresponding to forward production of π^+, π^-, $\pi^+ \pi^+$, $\pi^+ \pi^-$, or $\pi^+ \pi^+ \pi^-$ with the remaining particles in the backward hemisphere (the proton is rarely in the forward hemisphere and LPS regions with the proton forward were not considered). As expected, the regions to which the diffractive and exchange reactions contribute are the most highly populated.

Table VII lists the cuts and LPS region in which each was applied. The peripheral process which each cut was intended to remove is also listed. Since constituent interactions could also contribute to these LPS regions, care was taken to retain as many of these events as possible. Thus, in some regions only those events which displayed characteristics of the peripheral process were rejected. For instance, the invariant mass of the π^+ and proton in the backward hemisphere was required to be less than 1.4 GeV/c^2 for regions in which the exchange reaction produces a Δ^{++}. The combined effect of all the cuts was to remove 54% of the total number of events in the three reactions.

---

[a]Present address: Carolina Power and Light Co., Raleigh, NC 27602.
[b]Present address: SLAC, Stanford, CA 94305.
[c]Present address: Fermilab, Batavia, Illinois 60510.
[d]Present address: Purdue University, Lafayette, Indiana 47907.
[e]Present address: RCA, Fort Walton Beach, Florida 32548.
[f]Present address: NSPL Station, Bay St. Louis, Mississippi 39520.
[g]Present address: American Dade, Costa Mesa, CA 92626.
[h]Present address: Science Applications, Inc., Sunnyvale, CA 94089.
[i]Present address: Synergistic Development Ass., Mt. View, CA 94042.

[1]*Partons in Soft Hadronic Process,* proceedings of the Europhysics Study Conference, Greece, 1981, edited by Z. T. van de Walle (World Scientific, Singapore, 1981).
[2]K. Fiałkowski and W. Kittel, Rep. Prog. Phys. **46**, 1283 (1983).
[3]J. Whitmore, *Proceedings of the 19th International Conference on High Energy Physics, Tokyo, 1978,* edited by S. Homma, M. Kawaguchi, and H. Miyazawa (Physical Society of Japan, Tokyo, 1979), p. 63.
[4]R. K. Clark *et al.*, Phys. Rev. D **32**, 1061 (1985).
[5]M. Ferguson, Ph.D. dissertation, Duke University, 1984.
[6]N. Morgan, Ph.D. dissertation, Duke University, 1984.
[7]C. Baltay *et al.*, Phys. Rev. D **17**, 62 (1978).
[8]M. Deutschmann *et al.*, Nucl. Phys. **B103**, 426 (1976).
[9]The relativistic Breit-Wigner function is defined as

$$R_{\mathrm{BW}}(m) = \frac{m m_0 \Gamma}{(m^2 - m_0^2)^2 + m_0^2 \Gamma^2} ,$$

where $\Gamma = \Gamma_0 (q/q_R)^{2s+1}$, m_0 = mass of resonance, Γ_0 = width of resonance, $q = q$ value of resonance decay when mass is equal to m, $q_R = q$ value of decay when mass is equal to m_0, and s = spin of resonance. See also, J. D. Jackson, Nuovo Cimento **34**, 1644 (1964).
[10]Particle Data Group, Rev. Mod. Phys. **56**, S1 (1984).
[11]Table II contains the cross sections determined from our analysis of the untriggered data rather than those given in Ref. 7. The results reported therein used a polynomial to describe the entire background and a simple Breit-Wigner function for the resonance structure. We also did fits of this type, but better χ^2 per degree of freedom were obtained with the method described in Sec. II B. Thus, we consider our measurements more accurate and prefer them for this analysis.
[12]J. Bartke *et al.*, Nucl. Phys. **B118**, 360 (1977).
[13]T. K. Gaisser, F. Halzen, and E. A. Paschos, Phys. Rev. D **15**, 2572 (1977); F. Halzen, *Proceedings of the 21st International Conference on High Energy Physics,* Paris, 1982, edited by P. Petiau and M. Porneuf [J. Phys. (Paris) Colloq. **43**, C3-381 (1982)].
[14]P. D. B. Collins and A. D. Martin, *Hadron Interactions* (Hilger, London, 1984), p. 60.
[15]X. Artru, Phys. Rep. **97**, 147 (1983).
[16]B. Andersson *et al.*, Phys. Rep. **97**, 33 (1983).
[17]T. Sjöstrand, Comput. Phys. Commun. **27**, 243 (1982).
[18]L. van Hove, Nucl. Phys. **B9**, 331 (1969).
[19]E. A. De Wolf, in *Multiparticle Dynamics 1981,* proceedings of the XIIth International Symposium, Notre Dame, Indiana, edited by W. D. Shephard and V. P. Kenney (World Scientific, Singapore, 1982), p. 189; in *Multiparticle Dynamics 1982,* proceedings of the XIIIth International Symposium, Volendam, The Netherlands, edited by E. W. Kittel, W. Metzger, and A. Stergiou (World Scientific, Singapore, 1983), p. 471.